

BENCHMARK TESTS FOR STRONG GROUND MOTION PREDICTION METHODS USING STOCHASTIC GREEN'S FUNCTION METHOD



K. Kato & A. Morikawa

Kobori Research Complex, Inc., Tokyo, Japan

Y. Hisada

Kogakuin University, Tokyo, Japan

S. Ohno

Tohoku University, Sendai, Japan

A. Nobata

Obayashi Corporation Technical Research Institute, Kiyose, Japan

Y. Yamamoto

Technology Center, Taisei Corporation, Yokohama, Japan

A. Nozu

Port and Airport Research Institute, Yokosuka, Japan

H. Kawabe

Kyoto University Reactor Research Institute, Osaka, Japan

SUMMARY

We performed benchmark tests for strong motion simulation methods using Stochastic Green's function method. This method is widely used to generate strong ground motions in high frequency range. The purpose of this paper is to know the range of variation under the same source, path and site conditions. This benchmark tests consist of 6 steps. Simple point source models are used in Step 1, and extended sources are used in Step 2. In Steps 3 and 4, more complicated analytical conditions are considered. In the Steps 5 and 6, the Kanto sedimentary basin for the 1923 Kanto earthquake (M7.9) is considered as an actual source and structure model. All the results calculated by participants generally show good agreement to each other. Since random phases are used in generating time histories, synthesized amplitude shows variation in particular frequencies. When applying the Stochastic Green's function method, this variation should be in mind.

Keywords: Strong Ground Motion Prediction, Benchmark Test, Stochastic Green's Function Methods, Random phase

1. INTRODUCTION

Benchmark tests for the strong motion simulation methods using Stochastic Green's function method have been performed as three years project since 2009. This method is widely used to generate strong ground motions in high frequency range, and applied to simulate the input ground motions for designing aseismic buildings/structures. The purpose of this paper is to know the range of variation among synthesized results under the same source, path and site conditions, since random phases are used in generating time histories in this method.

This benchmark tests consist of 6 steps. Very simple point source models in homogeneous and two-layered subsurface structures are used in Step 1, and extended sources are used in Step 2. Radiation coefficient of the source is assumed to be frequency independent, and only *SH* wave is considered. Site amplification is calculated assuming normal incidence of *SH* wave. Six groups of researchers/engineers participated using their own methods/codes.

In Steps 3 and 4, more complicated analytical conditions are considered. Frequency dependent

radiation coefficient of the source is applied. Since oblique incidences of both SH and SV waves are considered, vertical component is also generated in addition to horizontal components. These two conditions are different in comparisons with Steps 1 and 2. Five groups of researchers/engineers participated.

In the Steps 5 and 6, the Kanto sedimentary basin for the 1923 Kanto earthquake (M7.9) is considered as an actual source and structure model. Variable slip model is characterized to two asperities and background regions. Strong ground motions from the asperity are synthesized in Step 5, and those from characterized source model are synthesized in Step 6. Four groups of researchers/engineers participated.

By comparing the synthesized strong motions submitted by participants, points to keep in mind when applying Stochastic Green's function method are summarized.

2. BENCHMARK TESTS OF STEPS 1 & 2

Very simple point source models are used in Step 1, and extended sources are used in Step 2. Figure 1 shows schematic figure of source configuration and location of calculation points. Table 1 shows analytical condition. As for the subsurface structure, Models S10 to S11 in Step 1 use half-space, and other models use two-layered structures shown in Table 2. Target frequency range is 1 to 20 Hz. Inelastic attenuation is not considered except for the Model S13. Only SH wave is considered.

Table 1. Lists of analytical condition for Step 1 (left) and Step 2 (right)

		Step 1 (Point source)				Step 2 (Extended source)			
Model		S10	S11	S12	S13	S21	S22	S23	
Subsurface structure		Half-spaced structure		Two-layered structure		Two-layered structure			
Q value		not considered			considered	not considered			
Source		Point source				Strike slip	Dip slip	Strike slip	
Rupture starting time						Constant		Random	
Target range		1~20 Hz				1~20 Hz			
Output		000, +002, +006, +010 (Total 4 points)				000, ±002, ±006, ±010 (Total 7 points)			
Random phase		Given	Individually generate 3 pattern			Individually generate 3 pattern			

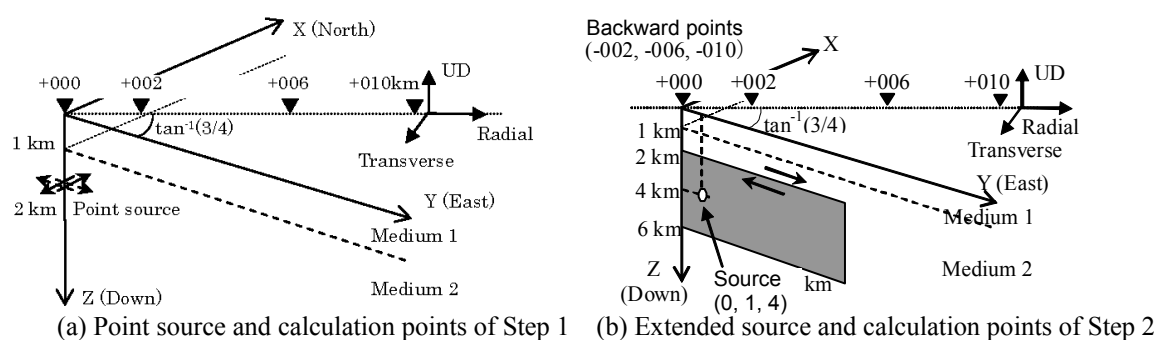


Figure 1. Schematic figure of source configuration

Table 2. Subsurface structure used in Steps 1 to 4

	Thickness (m)	Velocity		Density ρ (kg/m ³)	Q value	
		Vp (m/s)	Vs (m/s)		Qp	Qs
1st layer	1000	4000	2000	2600	40f ^{1.0}	40f ^{1.0}
2nd layer (Half space)	∞	6000	3464	2700	70f ^{1.0}	70f ^{1.0}

Generation of strong ground motions from the point source is based on Boore (1983). Acceleration spectrum, $A(\omega)$, at calculation points is expressed as follows,

$$A(\omega) = S(\omega) \cdot Z(\omega) \quad (1)$$

$$S(\omega) = \frac{F_S \cdot R_k^S \cdot P_{RTTN}}{4\pi\rho V_S^3} \{\omega^2 \dot{M}(\omega)\} \quad (2)$$

$$Z(\omega) = \frac{1}{r} \exp\left(-\frac{\omega \cdot r}{2V_S Q_S}\right) \quad (3)$$

where $S(\omega)$ is the source term, $Z(\omega)$ is the path term, and ω is the circular frequency. F_S is the site amplification coefficient, R_k^S is the radiation coefficient for S waves, P_{RTTN} is the reduction factor that accounts for the partitioning of energy into two horizontal components. ρ and V_S are the density and the shear velocity, and r is the distance. Q_S is the quality factor for S waves. R_k^S is 0.63, and assumed to be frequency independent. $\dot{M}(\omega)$ is the moment rate function expressed by

$$|\omega^2 \dot{M}(f)| = \frac{\omega^2 M_0}{1 + (f/f_c)^2} P(f, f_{\max}) \quad (4)$$

where M_0 is the seismic moment, and f_c is the corner frequency. P is the high-cut filter expressed by

$$P(f, f_{\max}) = \frac{1}{\sqrt{1 + (f/f_{\max})^{2n}}} \quad (5)$$

where n controls the decay rate at high frequencies. In Steps 1 and 2, we use $M_0=10^{18}\text{Nm}$, $V_S=3.464\text{km/s}$, $f_c=0.2\text{Hz}$, $f_{\max}=6\text{Hz}$, $n=4$. F_S is 2.0 for the half-space. In case of two-layered structures, F_S is calculated assuming normal incidence of SH wave.

Time series $w(t)$ are given by

$$w(t) = at^b e^{-ct} H(t) \quad (6)$$

where $H(t)$ is the Heaviside-step function, and coefficients a , b , c with $\varepsilon=0.2$ and $\eta=0.05$ are

$$a = \left(\frac{5\varepsilon}{T_w}\right)^b, \quad b = \frac{-\varepsilon \ln \eta}{1 + \varepsilon(\ln \varepsilon - 1)} \cong 1.25315, \quad c = \frac{b}{\varepsilon T_w} \cong \frac{6.2657}{T_w} \quad (7)$$

where $T_w=2/f_c$ (Boore, 1983). A number of acceleration time series satisfying the equation (6) are generated from random phases, and the best to third fit time series to the equation (2) are selected.

As examples of Step 1 benchmark tests, Figure 2(a) shows acceleration time series of the Model S11 at +010km point from 6 participants. Onset time of S waves and envelope of time series correspond each other, although phases show differences because random numbers are used to generate phases. Figure 2(b) and (c) show pseudo response spectra from two participants as examples, showing good agreement from the practical point of view.

The extended source, shown in Figure 1(b), is used in Step 2. Fault length, width, and rupture starting point are assumed to 8km and 4km, (0, 1, 4) km, respectively. Strike, dip, and slip angles of the fault are 90, 90, 180 degrees. M_0 , f_c , and rise time τ are $1.04 \cdot 10^{18}\text{Nm}$, 0.404Hz, and 5s, and other analytical conditions are described in Kato *et al.* (2011) in detail.

Strong motion synthesis is based on Irikura (1986). The strong motion of the extended source $U(t)$ is expressed using the strong motion of the sub-fault $u_{ij}(t)$.

$$U(t) = \sum_i \sum_j^{N_L N_W} u_{ij}(t - t_{ij}) + \sum_i \sum_j \sum_k^{N_D-1} \frac{1}{n'} u_{ij} \left\{ t - t_{ij} - \frac{(k-1)\tau}{(N_D-1)n'} \right\} \quad (8)$$

$$t_{ij} = \frac{r_{ij}}{V_r} + \frac{\eta_{ij}}{V_r} \quad (9)$$

where N_L , N_W , N_D are divided number of the extended source for length, width, and slip direction. V_r is rupture velocity, r_{ij} and η_{ij} are distance from the sub-fault to the calculation point, and from the rupture starting point to the sub-fault. n' is subdividing number to reduce artificial noise. M_o , f_c , and T_w of the sub-event are assumed to $5.4 \cdot 10^{15}$ Nm, 2.33 Hz, and 0.86 s, respectively. Using the scaling relation between the sub-fault and extended fault, N_L , N_W , N_D are determined to 8, 4, and 6.

Figure 3 shows acceleration time series of the Model S21 at -010, +000, and +010 points, and Figure 4 shows their pseudo velocity spectra. Time series of the forward direction (+010) show shorter duration than those of backward direction (-010) due to the rupture directivity effect. In the backward direction, the artificial predominant period at around 0.6 s is recognized caused by the regular intervals of the rupture times. To avoid the artificial predominant period, the random rupture times at the sub-faults, ε_{ij} is introduced (Irikura, 1986).

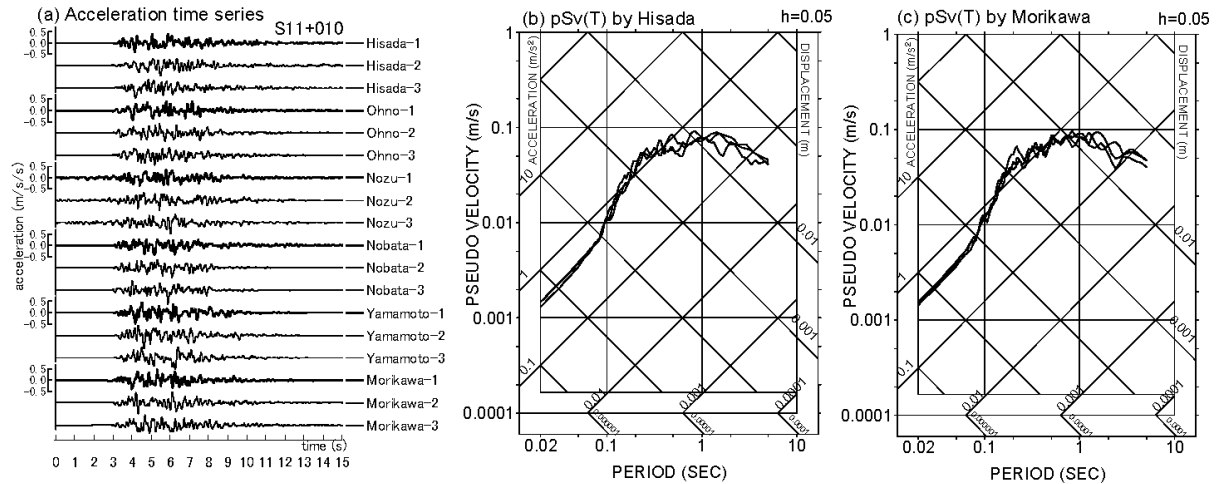


Figure 2. Acceleration time series and pseudo velocity spectra of the Model S11 at +010 point

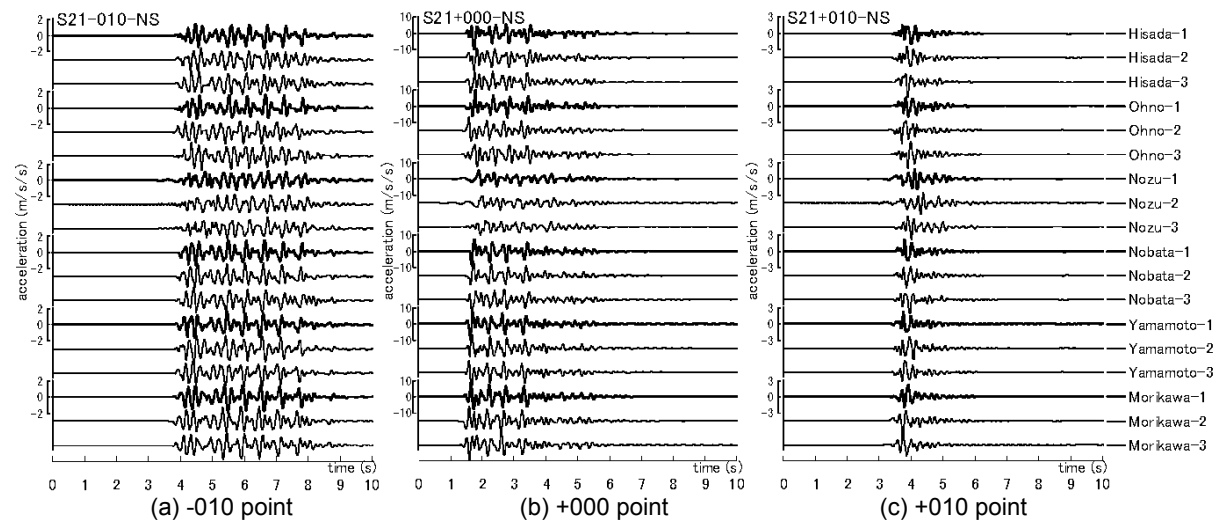


Figure 3. Acceleration time series of the Model S21 at (a) -010, (b) +000, and (c) +010 points

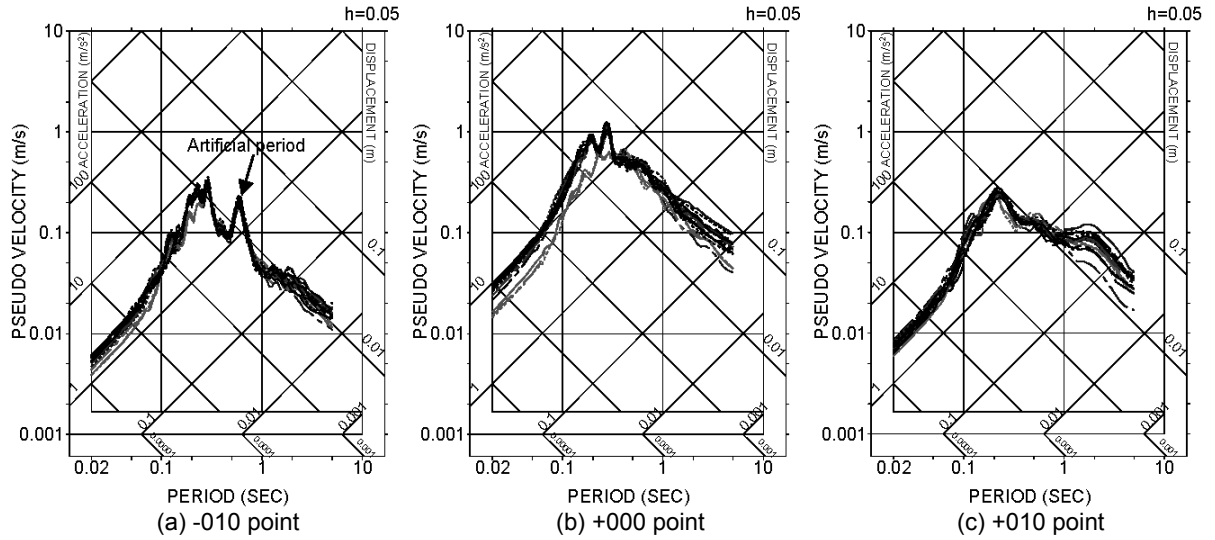


Figure 4. Pseudo velocity spectra of the Model S21 at (a) -010, (b) +000, and (c) +010 points

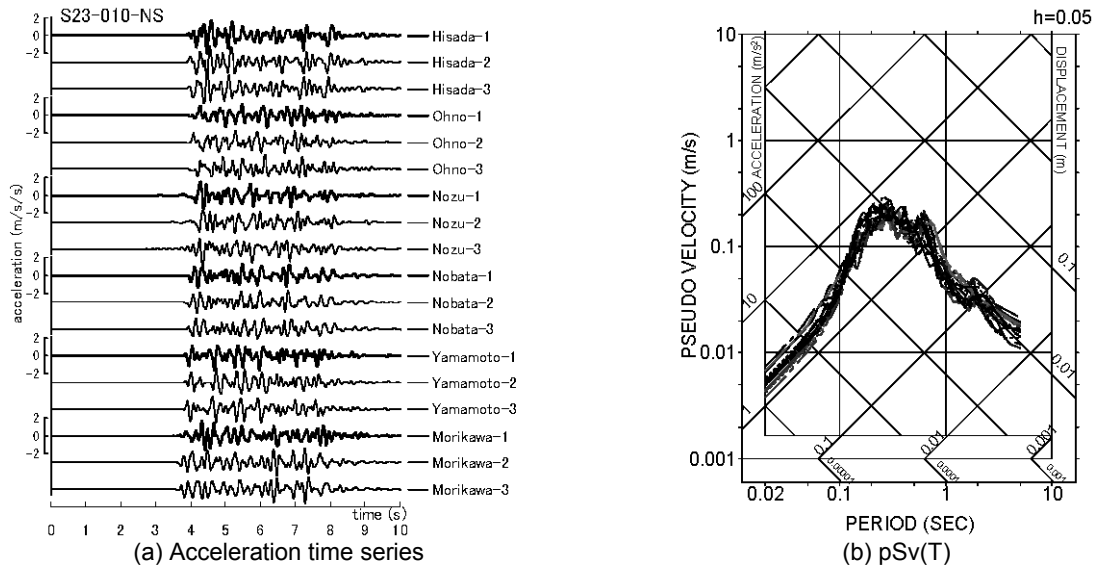


Figure 5. Acceleration time series and pseudo velocity spectra of the Model S23 at -010 point

$$t_{ij} = \frac{r_{ij}}{V_S} + \frac{\eta_{ij}}{V_r} + \varepsilon_{ij} \quad (10)$$

The revised time series and their pseudo velocity spectra are shown in Figure 5. This model corresponds to the Model S23. The artificial period disappeared and effectiveness of equation (10) is confirmed.

3. BENCHMARK TESTS OF STEPS 3 & 4

In Steps 3 and 4, frequency dependent radiation coefficient of the source and oblique incidences of both SH and SV waves are applied. Step 3 uses the point source and Step 4 uses extended source those are the same models as Steps 1 and 2. Table 3 shows analytical condition. Since oblique incidences of SV waves are considered, vertical component is also generated in addition to horizontal components. Random phases are independently given to SH and SV waves. Other analytical conditions are described in Kato *et al.* (2012) in detail. As an example of point source test, Figure 6 shows acceleration time series and pseudo velocity spectra of the Model S33 at +010 point.

Table 3. Lists of analytical condition for Step 3 (left) and Step 4 (right)

	Step 3 (Point source)				Step 4 (Extended source)				
Model	S31	S32	S33	S34	Model	S41	S42	S43	S44
Subsurface structure	Half-spaced	Two-layered structure		Four-layered	Subsurface structure	Two-layered structure			
Incident angle	Normal	Oblique			Incident angle	Oblique			
Q value	no	considered			Q value	considered			
Source	Point source				Source	Strike slip	Dip slip	Strike slip	
Radiation (SH & SV)	Frequency independent		Frequency dependent		Radiation (SH & SV)	Frequency dependent			arbitrarily
Rupture starting time	0~20 Hz				Rupture starting time	Constant	Random	Constant	
Target range					0~20 Hz				Target range
Output	000, +002, +006, +010 (Total 4 points)				Output	000, ±002, ±006, ±010 (Total 7 points)			
Component	Horizontal	Horizontal and vertical			Component	Horizontal and vertical			
Random phase	Individually generate 3 pattern				Random phase	Individually generate 3 pattern			

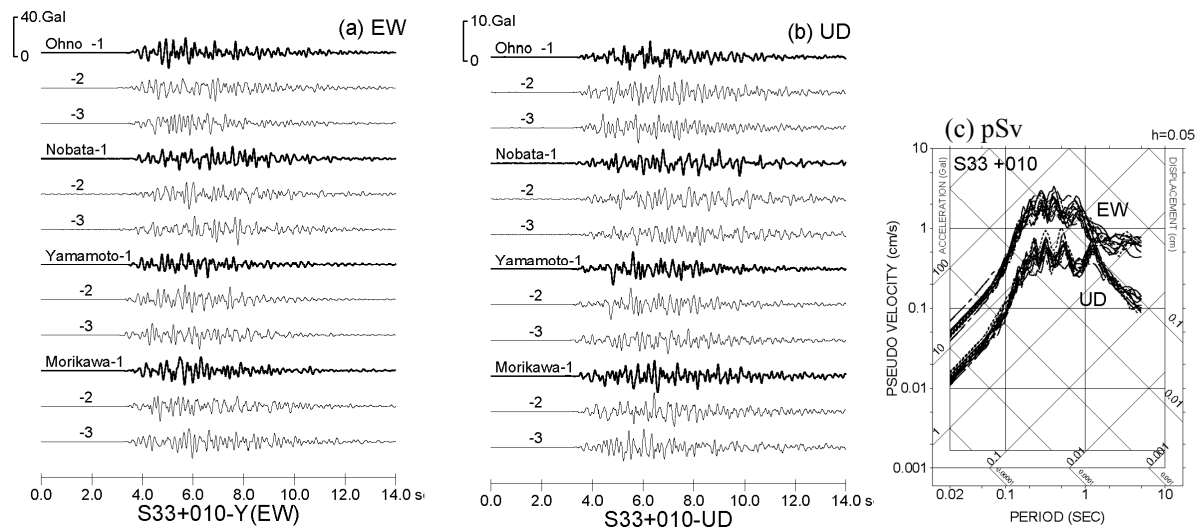


Figure 6. Acceleration time series and pseudo velocity spectra of the Model S33 at +010 point

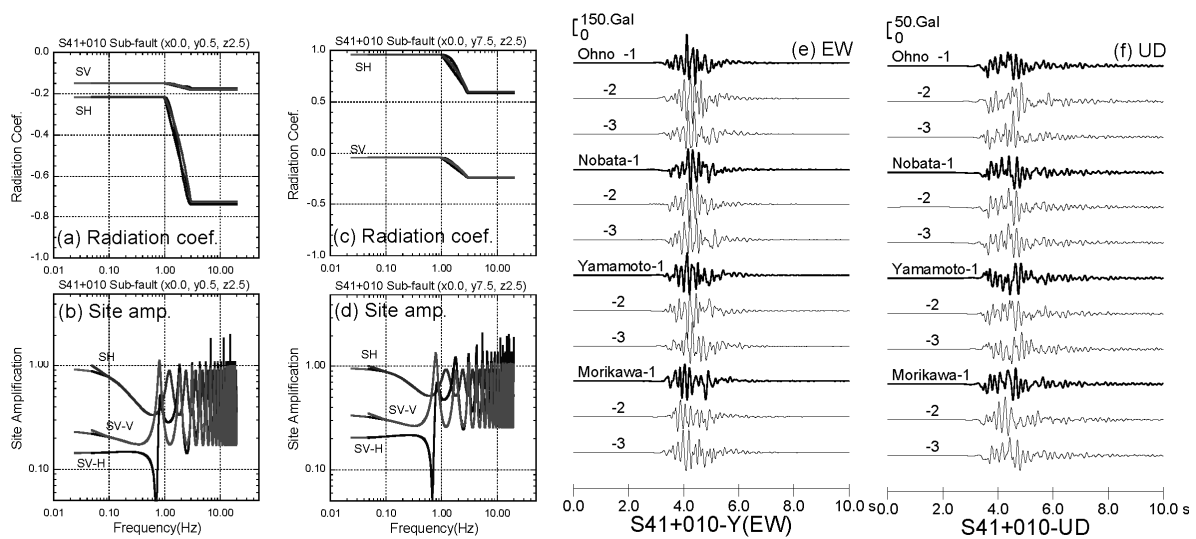


Figure 7. Comparison of radiation coefficients, site amplification factor, and acceleration time series of the Model S41 at +010 point

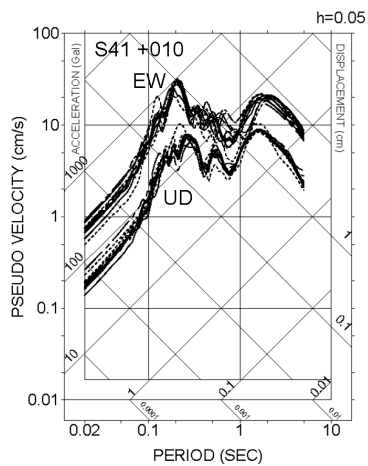


Figure 8. Pseudo velocity spectra of the Model S41 at +010 point

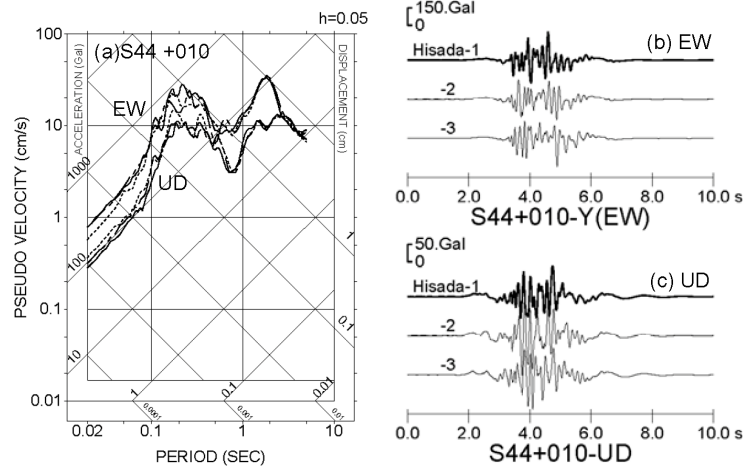


Figure 9. Pseudo velocity spectra and acceleration time series of the Model S44 at +010 point

Following Pitarka *et al.* (2000), theoretical radiation coefficient is applied for the frequency range lower than 1 Hz and the smoothed radiation is applied for the range higher than 3 Hz. The frequency range from 1 to 3 Hz is transition zone. The incident angle from the point source to the +010 point exceeds the critical angle of 35 degree. In spite of such complicated analytical conditions, the envelope of time series and the response spectra from four participants correspond to each other.

As an example of extended source test, Figure 7 shows the results of the Model S41 at +010 point. From each sub-fault to the calculation point, different site amplification factors and different frequency dependent radiation coefficients are applied. Since this analytical condition is more complicated than Step 3, we check the factors from participants in advance. Figures 7(a) and (b) show comparison of radiation and site amplification factors from upper left sub-fault shown in Figure 1(b), Figures 7(c) and (d) show those from upper right sub-fault. We confirm that these factors show good agreement each other. Figure 8 shows pseudo velocity spectra calculated from time series shown in Figures 7(e) and (f). Since the radiation and site amplification factors coincide with each other, it is suggested that the variation shown in response spectra is mainly originated from random phases.

The Model S44 is an option case that participants can use their own method. Co-author Hisada joined S44 by applying exact Green's function based on the wavenumber integral method (Hisada, 2008) which can treat full wave field. Figure 9 shows pseudo velocity spectra and acceleration time series of the Model S44 at +010 point. Since both Models S41 and S44 use theoretical radiation coefficient in the period range longer than 1 s, we can directly compare the spectra in Figures 8 and 9(a) each other. We can find that predominant period can be commonly recognized at 2 s in EW component. On the other hand, the spectral of S44 at around 2 s in UD component shows larger amplitude than that of S41. We can also find long period phase on time series at around 6 s in Figure 9(c). This difference stems from the excitation of surface wave, which can't be considered in Stochastic Green's function method.

4. BENCHMARK TESTS OF STEPS 5 & 6

In the Steps 5 and 6, as an actual source model, the 1923 Kanto earthquake (M7.9) is considered and the Kanto sedimentary basin is used as structure model. Table 4 shows analytical condition. Figure 10 shows the fault model of the 1923 Kanto earthquake, and location of 4 stations, ASK on rock site, KYS, ECJ, and JSK on sediment sites. Layered half space beneath each site is used for calculations of which subsurface structure comes from the 3D Kanto basin model (http://www.jishin.go.jp/main/chousa/09_choshuki/dat/index.htm). Variable slip model by Sato *et al.* (2005) is characterized into two asperities and background regions, as shown in Figure 10, based on the idea by Dan *et al.* (2002). Table 5 shows characterized fault parameters of the 1923 Kanto earthquake. Strong ground

motions from the point source within the asperity 2 are synthesized in Step 5, and those from characterized source model are synthesized in Step 6.

Step 5 assumes the point source with frequency dependent radiation pattern, and oblique incidences of SH and SV waves are considered. M_o , f_c , and f_{max} are $8.0 \cdot 10^{18}$ Nm, 0.15 Hz, 13.5 Hz respectively. As an example of the results of the Model S51, Figure 11 shows acceleration time series and pseudo velocity spectra at ASK offered by 4 participants. Since random phases in generating time histories are given in advance in S51, synthesized strong ground motions show almost perfect agreement. This agreement indicates that the frequency dependent radiation coefficient of the source is properly applied, and site response by oblique incidences of both SH and SV is accurately calculated.

Figure 12 shows the results of the Model S52. Since random phases are individually generated by participants, acceleration time series and pseudo velocity spectra show variation in comparison with Figure 11. This kind of variation is inevitable as far as Stochastic Green's function method is used.

In Step 6, the characterized fault model is applied. The size of sub-fault is 13 km in length and 10 km in width, and rise time is assumed from 12.6 to 13.8 s based on Sato *et al.* (2005). As an example of the results of the Model S61, Figure 13 shows acceleration time series and pseudo velocity spectra at ASK offered by 4 participants. Onset time of S waves and envelope of time series correspond to each other. In Figure 13(b), response spectrum from the empirical attenuation model by Nishimura *et al.* (2001) is also shown. The spectra from Stochastic Green's function method and that from the empirical attenuation model show good agreement in the period range shorter than 0.5 s. On the contrary, the spectra from Stochastic Green's function method are underestimated in the range longer than 0.5 s.

Table 4. Lists of analytical condition for Step 5 and Step 6

Model	Step 5 (Point source)		Step 6 (Extended source)	
	S51	S52	S61	S62
Target	2nd asperity of the 1923 Kanto earthquake (Mj7.9)		The 1923 Kanto earthquake (Mj7.9)	
Fault model	One sub-event within 2nd asperity		Characterized fault model based on Sato <i>et al.</i> (2005)	Slip model by Sato <i>et al.</i> (2005)
Subsurface structure	Layered half space beneath the site of which subsurface structure comes from 3D Kanto basin model			
Q value	Considered			
Random phase	Given	Individually generate 3 patterns		
Target frequency	0~20Hz			
Output	4 sites (Rock site: ASK, Sediment site: KYS, JSK, ECJ)			

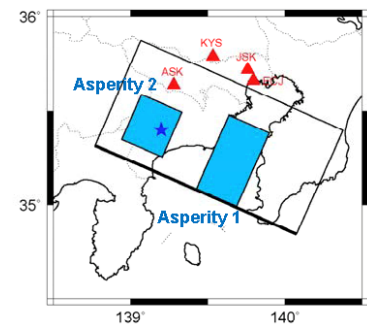


Figure 10. Characterized fault model and location of stations

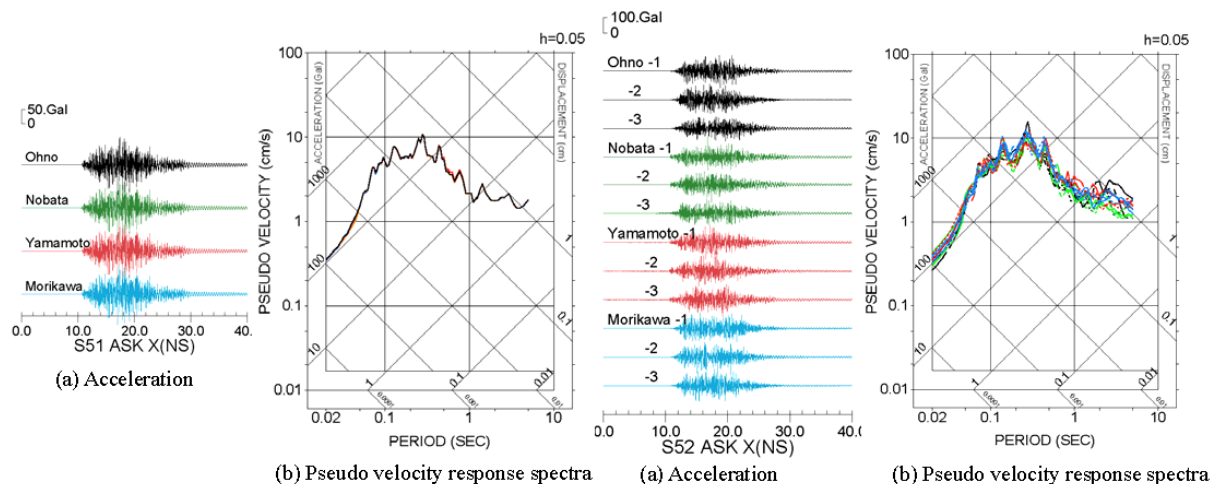


Figure 11. Acceleration time series and pseudo velocity spectra of the Model S51 at ASK

Figure 12. Acceleration time series and pseudo velocity spectra of the Model S52 at ASK

It is suggested that the setting of longer rise time is one of the reason why the amplitude of spectra longer than 0.5s is relatively small. When we find the discrepancy between the results of two different methods, we had better re-examine the validity of fault parameters. This kind of re-examination would improve the result of Stochastic Green's function method.

Table 5. Fault parameters of the 1923 Kanto earthquake

Fault Parameter		Value	Unit	
Outer parameter	Strike	294°		
	Dip	16°		
	Rupture velocity	3.0	km/s	
	Rupture direction	Circular		
	Stress drop	2.8	MPa	
	Rigidity	3.00E+10	N/m ²	
	Area	9100	km ²	
	Seismic moment	9.94E+20	Nm	
	Average slip	364	cm	
S-wave velocity	3.53	km/s		
Inner parameter	Asperity (Total)	Seismic moment	4.54E+20	Nm
		Area	2080	km ²
		Average slip	728	cm
		Stress drop	5.1	MPa
		Hi-frequency level	2.07E+19	Nm/s ²
	1st asperity (Around Miura peninsula)	Seismic moment	3.1007E+20	Nm
		Area	1300	km ²
		Average slip	795	cm
		Stress drop	5.1	MPa
		Hi-frequency level	1.63E+19	Nm/s ²
	2nd asperity (Around Odawara city)	Seismic moment	1.4411E+20	Nm
		Area	780	km ²
		Average slip	616	cm
		Stress drop	5.1	MPa
		Hi-frequency level	1.27E+19	Nm/s ²
Background	Seismic moment	5.3933E+20	Nm	
	Area	7020	km ²	
	Average slip	256	cm	
	Stress drop	1.8	MPa	
	Hi-frequency level	1.34E+19	Nm/s ²	

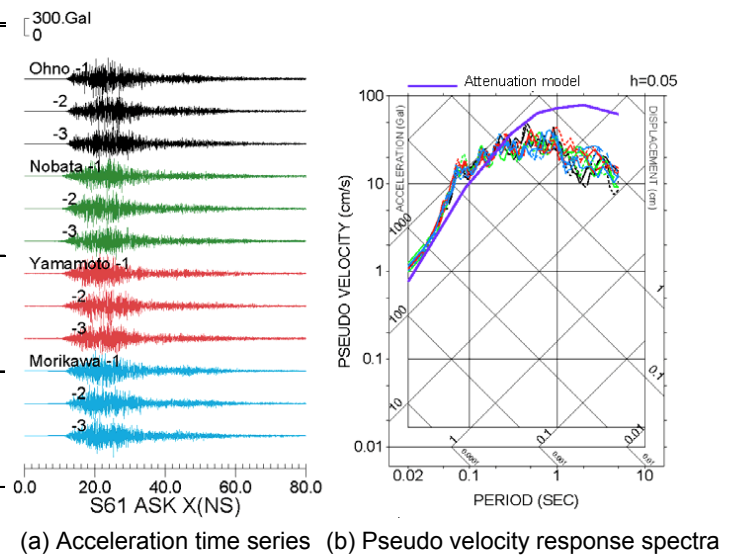


Figure 13. Acceleration time series and pseudo velocity spectra of the Model S61 at ASK

5. COCLUSIONS

We performed benchmark tests for strong motion simulation methods using Stochastic Green's function method, in order to know the range of variation under the same source, path and site conditions. All the results calculated by participants generally show good agreement to each other, in spite of complicated analytical condition such as oblique incidence of *SH* and *SV* waves and use of frequency dependent radiation coefficients. Since random phases are used in generating time histories, synthesized amplitude shows variation in particular frequencies. When applying the Stochastic Green's function method, this variation should be in mind.

ACKNOWLEDGEMENT

This work was supported by Grant-in-Aid for Scientific Research (B) of MEXT (Japan Ministry of Education, Culture, Sports, Science and Technology), and Research Centre of Urban Disaster Mitigation (UDM) in Kogakuin University. We also thank Prof. R. Kobayashi of Kagoshima University for providing their source parameters and Sub-Committee on Strong Motion Observation of Architectural Institute of Japan for providing the strong motion data.

REFERENCES

- Boore, D. M. (1983). Stochastic simulation of high-frequency ground motion based on seismological models of the radiated spectra, *Bulletin of Seismological Society of America*, **73**, 1865-1894.
- Dan, K., Miyakoshi, J. and Yashiro, K. (2002). Simlation of ground motions at Sapporo and Akita during the 1993 Hokkaido-Nansei-Oki earthquake by empirical Green's function method -Verification of characterizing procedure of earthquake source model for strong motion prediction-, *J. Struct. Constr. Eng., AIJ*, No.554, 53-62 (in Japanese with English abstract).

- Hisada, Y. (2008). Broadband strong motion simulation in layered half-space using stochastic Green's function technique, *Journal of Seismology*, **12**, No.2, 265-279.
- Irikura, K. (1986). Prediction of strong acceleration motions using empirical Green's function, *Proc. 7th Japan Earthquake Engineering Symposium*, 151-156.
- Kato, K., Hisada, Y., Kawabe, H., Ohno, S., Nozu, A., Nobata, A., Morikawa, A. and Yamamoto, Y. (2011). Benchmark tests for strong ground motion prediction methods: Case for Stochastic green's function method (Part 1), *AIJ J. Technol. Des.* Vol. **17**, No.35, 49-54 (in Japanese with English abstract).
- Kato, K., Hisada, Y., Ohno, S., Nobata, A., Morikawa, A. and Yamamoto, Y. (2012). Benchmark tests for strong ground motion prediction methods: Case for Stochastic green's function method (Part 2), *AIJ J. Technol. Des.* Vol. **18**, No.38, 67-72 (in Japanese with English abstract).
- Nishimura, I., Noda, S., Takahashi, K., Takemura, M., Ohno, S., Tohdo, M. and Watanabe, T. (2001). Response spectra for design purpose of stiff structures on rock sites, *Transactions of SMiRT 16*, Paper #1133, 1-8.
- Pitarka, A., Somerville, P., Fukushima Y., Uetake, T. and Irikura, K. (2000). Simulation of near-fault strong-ground motion using hybrid Green's functions, *Bulletin of Seismological Society of America*, **90**, 566-586.
- Sato, H., Hirata, N., Koketsu, Okaya, K., Abe, Kobayashi, R., Matsubara, M., Iwasaki, T., Ito, T., Ikawa, T., Kawanaka, T., Kasahara, K. and Harder S. (2005). Earthquake source fault beneath Tokyo, *Science*, **309**, 462-464.